

SEDIMENT CONCENTRATION BELOW FREE OVERFALL

By O. R. Stein,¹ Associate Member, ASCE,
and P. Y. Julien,² Member, ASCE

ABSTRACT: Time-varying sediment concentration exiting a plunge pool is analyzed by considering the effect of free-overfall jet diffusion on sediment detachment and scour. The analysis results in dimensionless relationships between scour volume, sediment concentration, maximum scour depth, and time. Sediment concentration is at a maximum near the initiation of scour, when the eroding bed is at the tip of the impinging jet's potential core. Thereafter, sediment concentration decreases as a function of time and scour-hole geometry, expressed as maximum scour depth. Dimensionless geometric relationships show that the scour volume per unit width can be expressed as twice the square of the maximum scour depth at the corresponding time for the cohesive and noncohesive soils tested. Analytical relationships between sediment concentration and time are verified by laboratory experiments of scour below a free overfall on two sand-bed materials (one coarse and one fine) and on one cohesive soil, each replicated several times. The agreement between measured and predicted values is best for the noncohesive sands.

INTRODUCTION

A free overfall is associated with an abrupt break in channel bed slope such as below grade-control structures, dam outlets, cantilevered pipes, and head cuts incised in ephemeral streams. The scour potential in the region immediately downstream from the free overfall is well documented. For example, Bormann and Julien (1991) have examined scour below grade-control structures; Blaisdell and Anderson (1988a,b) studied the scour potential below cantilevered pipes; Holland and Pickup (1976), Begin et al. (1980a,b), Gardner (1983), and Stein and Julien (1993) examined the sediment production and migration of head cuts. A summary of an empirical approach for the analysis of scour below hydraulic structures is provided by Mason and Arumugam (1985). Scour dimensions have also been related to impinging-jet diffusion (Kobus et al. 1979; Rajaratnam 1981, 1982; Chee and Yuen 1985). Most research efforts have focused on predicting scour depth, which may affect the structure at the free overfall, as opposed to volumetric scour dimensions and sediment concentration, which may affect downstream morphology and water quality as well as the structure but are much more difficult to measure in an actively eroding plunge pool.

The aim of this paper is to determine relationships between time, scour depth, scour-hole volume, and sediment concentration generated by flow at a free overfall, independent of possible soil mass wasting contributions to downstream sediment load. The analysis describes the change with time of sediment detachment and transport within a developing plunge pool at the soil/water interface. The approach relates downstream sediment con-

¹Asst. Prof., Dept. of Civ. and Agric. Engrg., Montana State Univ., Bozeman, MT 59717.

²Assoc. Prof., Dept. of Civ. Engrg., Colorado State Univ., Fort Collins, CO 80523.

Note. Discussion open until February 1, 1995. To extend the closing date one month, a written request must be filed with the ASCE Manager of Journals. The manuscript for this paper was submitted for review and possible publication on May 23, 1993. This paper is part of the *Journal of Hydraulic Engineering*, Vol. 120, No. 9, September, 1994. ©ASCE, ISSN 0733-9429/94/0009-1043/\$2.00 + \$.25 per page. Paper No. 6224.

centration to diffusion of an impinging jet. Jet diffusion is used to determine the time change in maximum scour depth. In turn, dimensionless relationships between scour depth and volume are developed. Finally, sediment concentration rate is related to scour volume changes. The analysis results in graphic relationships between sediment concentration and time. These relationships are tested using laboratory measurements of sediment concentration leaving a scour hole created by the impingement of a free overfall jet on three bed materials: two relatively uniform sand sizes and one cohesive soil.

JET DIFFUSION AND SCOUR HOLE GEOMETRY

The plunge pool created by the impingement of a two-dimensional plane jet on an erodible bed, as produced below a free overfall, is shown in Fig. 1. The jet, with an origin at the water surface and initial thickness y_0 , enters the plunge pool at an angle χ and nearly uniform average velocity U_0 . Free jets, unaffected by a boundary, spread longitudinally and diffuse throughout the surrounding fluid, decreasing in average velocity as analyzed by Albertson et al. (1950). The zone in which the centerline velocity remains constant at U_0 defines the potential core, of length J_p from the jet origin. Beyond this distance, the velocity U remains a maximum along the jet centerline but the entire flow velocity field is reduced by diffusion.

The generally accepted formulation for the centerline velocity U where $J > J_p$ (Rajaratnam 1976) is:

$$\frac{U}{U_0} = C_d \sqrt{\frac{y_0}{J}}; \quad J > J_p \quad (1)$$

where J = the distance from the origin along the centerline, and the diffusion constant $C_d \approx 2.47$ is similar to the value (≈ 2.28) suggested by Albertson et al. (1950). Turbulence and nonuniform flow velocity at the jet origin

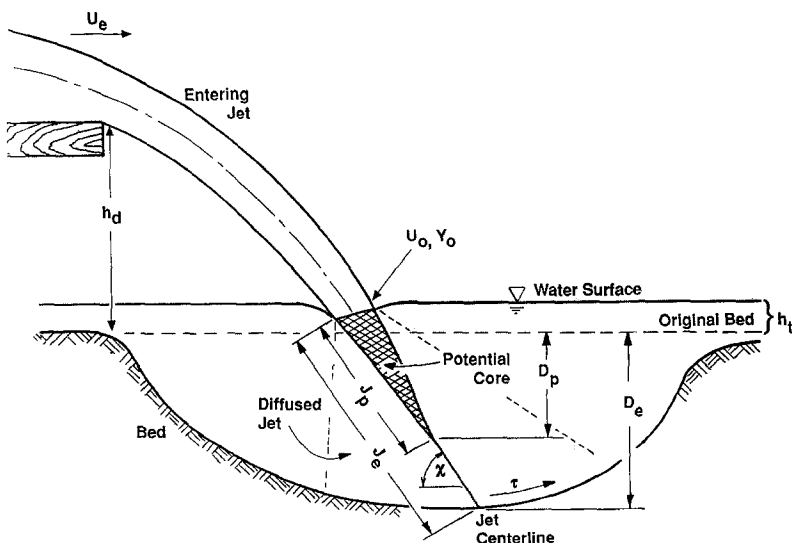


FIG. 1. Plunge-Pool Definition

influences both C_d and J_p . The length of the potential core can be obtained by solving (1) when $U = U_0$ at $J = J_p$:

$$J_p = C_d^2 y_0 \quad (2)$$

Impinging jets, deflected by a flat impervious boundary, were analyzed by Beltaos (1972, 1974). His results for plane jets (Beltaos and Rajaratnam 1973; Beltaos 1976) identify three distinct regions in an impinging jet. The flow is analogous to a free jet for some distance from the origin and analogous to a wall jet beyond some longitudinal distance along the boundary from impingement. Between these regions, the jet is deflected by the boundary, causing the velocity streamlines to curve and an excess static pressure to develop. Beltaos defined the impingement region as the region in which streamlines resemble neither a free nor wall jet. His expressions for the maximum velocity in the free jet and impingement regions can be converted to the form of (1) in which only the value of the coefficient C_d varies. These values are 2.50 in the free-jet region and 2.72 in the impingement region, suggesting that an impervious boundary increases the effective diffusion constant.

Scour-hole geometry is usually represented by maximum depth:

$$D = J \sin \chi - h_t \quad (3)$$

where D = the maximum depth at an arbitrary time; and h_t = the tailwater depth. Many studies have found that other scour-hole dimensions can be related to depth (Chee and Kung 1971; Rajaratnam 1981; Blaisdell et al. 1981; Blaisdell and Anderson 1988b). Rouse (1940) first suggested that scour depth increases linearly with the log of the time. This approximation assumes that the scour depth increases infinitely with time and invalidates the concept of equilibrium or ultimate scour depth. Laursen (1952) convincingly argued for the concept of equilibrium scour depth using the Shields parameter threshold. At some time, however long, the scour hole will have eroded to the point that the shear stress of the diffused jet equals the critical shear stress of the bed material. This analysis of course ignores the effect on scour of turbulent bursts, which as Robinson (1989a,b) reports may be an order of magnitude higher than the time-averaged shear stress.

ANALYTICAL DEVELOPMENT

Scour Depth versus Time

The sediment detachment rate per unit area E (mass/time/area) at the point of maximum scour can be determined from sediment continuity as the product of sediment bulk density B (mass of solids/total volume) and the change in scour depth D with time t . An excess shear equation is often used to determine the detachment rate in erosion models (Foster et al. 1977). Equating sediment continuity with the excess shear equation yields:

$$E = B \frac{dD}{dt} = \kappa(\tau - \tau_c)^\xi \quad (4)$$

where τ = the applied shear stress; τ_c = the critical shear stress of the bed material; and κ and ξ = experimentally determined constants.

The maximum shear stress τ acting on the bed in the scour hole can be related to the maximum diffused jet velocity in the plunge pool U by introducing a coefficient of friction C_f .

$$\tau = C_f \rho U^2 \quad (5)$$

Combining (1) and (5), with consideration of (2), gives the maximum applied bed shear stress τ , which within the potential core is constant at $\tau = \tau_0$:

$$\tau_0 = C_f \rho U_0^2; \quad J \leq J_p \quad (6)$$

$$\tau = C_d^2 C_f \rho U_0^2 \frac{y_0}{J}; \quad J > J_p \quad (7)$$

where J = the distance along the jet centerline from tailwater impingement to the eroding bed; J_p = the length of the jet potential core; U_0 and y_0 = the jet velocity and jet thickness at tailwater impingement; C_d = the diffusion coefficient, and C_f = the friction coefficient. The equilibrium scour depth D_e occurs when $\tau = \tau_c$; therefore, from (3) and (7), and assuming tailwater depth is insignificant ($h_t \approx 0$):

$$D_e = \frac{C_d^2 C_f \rho U_0^2 y_0}{\tau_c} \sin \chi \quad (8)$$

Similarly, from (2) and (3), the depth of scour when the bed is just at the tip of the potential core D_p is:

$$D_p = C_d^2 y_0 \sin \chi \quad (9)$$

From (3), (4), (6), (7), and (9), and assuming $h_t \ll D_e$, a nonlinear ordinary differential equation, applicable when the bed is beyond the potential core, is obtained:

$$\frac{dD}{dt} = \frac{\kappa}{B} \left(\frac{\tau_0 D_p}{D} - \tau_c \right)^\xi; \quad D \geq D_p \quad (10)$$

Integration of (4) from $t = 0$ to $t = T_p$ with τ constant at τ yields the time of potential core scour, which corresponds to the depth $D = D_p$:

$$T_p = \frac{B D_p}{\kappa (\tau_0 - \tau_c)^\xi} \quad (11)$$

The equilibrium scour depth D_e is obtained when the time change in scour depth is zero; thus from (10):

$$\frac{D_e}{D_p} = \frac{\tau_0}{\tau_c} \quad (12)$$

The time T_p and corresponding depth D_p delineate the break between potential core hydraulics and jet-diffusion hydraulics control of sediment detachment. For shorter times and shallower depths, when the bed is within the potential core, the scour rate [(4)] is independent of time because shear stress is constant [(6)]. Thereafter, as scour depth increases, shear stress [(7)] and scour rate [(10)] decrease. The scour rate beyond the potential core [(10)] can be rewritten in a dimensionless form:

$$\frac{dD^*}{dT^*} = \left(\frac{1 - D^*}{D^*} \right)^\xi; \quad D^* \geq D_p^* \quad (13)$$

by combining (10) and (12) and introducing dimensionless depths $D^* =$

D/D_e and $D_p^* = D_p/D_e$, and dimensionless time $T^* = t/T_r$, where T_r is a reference time of convenience with no physical significance, formulated by combining the dimensional hydraulic and sediment parameters of (10):

$$T_r = \frac{BD_e}{\kappa\tau_0^\xi} \left(\frac{D_e}{D_p} \right)^\xi = \frac{BD_e}{\kappa\tau_c^\xi} \quad (14)$$

Eq. (13) shows that the change in scour depth with time can be expressed as function of the ratio of maximum scour depth at the corresponding time to the equilibrium scour depth. Solutions to (13), in terms of T^* versus D^* , are dependent on value of the sediment-detachment exponent ξ . For values of $\xi = 1.0$ and 1.5 , respectively, solutions are (Stein et al. 1993):

$$T^* - T_p^* = -D^* - \ln(1 - D^*) \Big|_{D_p^*} \quad (15a)$$

$$T^* - T_p^* = (D^* - D_p^{*2})^{0.5} \left(1 - \frac{2}{D^* - 1} \right) - 1.5 \arcsin(2D^* - 1) \Big|_{D_p^*} \quad (15b)$$

where $T_p^* = T_p/T_r$ = the dimensionless time of potential core scour. The exponent value $\xi = 1.5$ is based on sediment transport equations and applicable to noncohesive-sediment detachment. Recent studies (Nearing et al. 1989; Hanson 1989; Stein and Julien 1991) on cohesive-soil detachment have suggested or measured a value of $\xi = 1.0$.

Sediment Concentration versus Scour Volume, Scour Depth, and Time

Owing to the conservation of mass, the sediment concentration leaving the two-dimensional scour hole can be expressed as the change in scour volume with time:

$$C = \frac{B}{\rho q} \frac{dV}{dt} \quad (16)$$

where C = the sediment concentration (mass solids/mass water); B = the bed-material bulk density; V = the scoured volume per unit width; ρ = the fluid mass density; q = the unit flow rate; and t = the time from the initiation of scour. Substituting the dimensionless $T^* = t/T_r$, and $V^* = V/D_e^2$ into (16) yields:

$$C = \frac{\kappa D_e \tau_c^\xi}{\rho q} \frac{dV^*}{dT^*} \quad (17)$$

where D_e = the equilibrium scour depth; κ and ξ = experimental sediment detachment parameters; and τ_c = the critical shear stress of the bed material.

A power function relating scour volume and scour depth $V^* = \alpha D^{*\beta}$ where α and β are experimentally determined constants yields:

$$\frac{dV^*}{dT^*} = \phi D^{*(\beta-1)} \frac{dD^*}{dT^*} \quad (18)$$

where $\phi = \alpha \cdot \beta$ = a scour-hole shape function; and $D^* = D/D_e$.

Sediment concentration and scour depth are then related by combining (13), (17) and (18):

$$C = \frac{\kappa D_e \tau_c^\xi}{\rho q} \phi D_p^{*(\beta-1)} \left(\frac{1 - D^*}{D_p^*} \right)^\xi, \quad D^* \geq D_p^* \quad (19)$$

The maximum sediment concentration occurs when scour is within the potential core, when $D^* = D_p^*$; thus from (19):

$$C_{\max} = \frac{\kappa D_e \tau_c^\xi}{\rho q} \phi D_p^{*(\beta-1)} \left(\frac{1 - D_p^*}{D_p^*} \right)^\xi \quad (20)$$

Defining $C^* = C/C_{\max}$, combination of (19) and (20) yields:

$$C^* = \frac{C}{C_{\max}} = \left(\frac{D_p^*}{D^*} \right)^{1+\xi-\beta} \left(\frac{1 - D^*}{1 - D_p^*} \right)^\xi, \quad D^* \geq D_p^* \quad (21)$$

Eqs. (19)–(21) show that the sediment concentration leaving the scour hole is a function of the corresponding normalized scour depth D^* , the scour-hole geometry through the shape function ϕ and the sediment-detachment potential of the flow. Of primary interest is the relationship between sediment concentration and time, achieved by combining (15) and (21). Graphic solutions to (15) and (21), comparing C^* and T^* as well as the relationship between scour volume and scour depth expressed in (18) are tested using laboratory data of scour below a free overfall for two different-sized noncohesive soils and one cohesive soil.

EXPERIMENTS

Several laboratory experiments were conducted in the Hydraulics Laboratory at Colorado State University to test the theoretical relationships developed in the previous section. An impinging jet was created by a free overfall at the end of a 100.0-cm-long acrylic-plastic plate set within an acrylic-plastic flume 10.4 cm wide by 200.0 cm long and 33.0 cm high. The flume was set at 3.7% slope for all experimental runs. Each run on a given bed material represents a unique jet configuration determined by varying either the discharge or drop height between the acrylic-plastic plate and erodible bed test section. Discharge was controlled by a pressure regulator and measured by a turbine meter in the nonrecirculating flume supply line. Drop height was controlled by placement of a nonerodible plate in the bed material downstream from the 40.0-cm test section. There was a smooth transition between the test bed and plate; therefore tailwater depth was the normal flow depth in the downstream section.

Two-dimensional scour profiles from a jet impinging on three different saturated bed materials were measured in the flume at sequential times throughout the scour process. Eight runs (14–21) on a coarse sand with a mean diameter d_{50} of 1.5 mm, six runs (22–27) on a fine sand $d_{50} = 0.15$ mm, and nine runs (3–13) on a cohesive soil $d_{50} = 0.045$ mm were conducted. The particle size distribution of each material is given in Fig. 2. The cohesive soil is a typical agricultural soil (Norka series) collected in eastern Colorado. To maintain uniform cohesive-soil conditions and to remove large pieces of organic matter, the air-dried soil was passed through a 0.420-mm sieve, which destroyed large aggregates but allowed the soil to retain cohesive properties upon rewetting.

The setup procedure for each run consisted of filling the flume test section including a volume underneath the upstream acrylic-plastic plate with the desired bed material in 5-cm layers. The bed material was then slowly

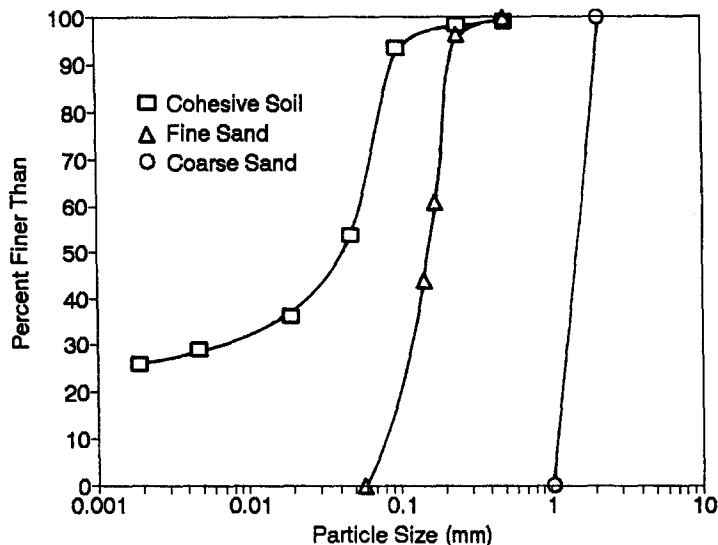


FIG. 2. Bed-Particle-Size Distribution

saturated from the bottom up. This method produced a uniform bulk density and water content for each bed material.

Bed profiles were measured using a photographic technique. A translucent acetate imprinted with a millimeter grid was adhered to the flume sidewall. An approximate 35 by 22 cm area of the test section was photographed through the acetate at intervals ranging from 5 s at initial times to 10 min at the longest times, depending on the rate of profile change. Typically, 30–40 profiles were taken per run. The profile photographs were digitized to store their x -, y -, and t -coordinates. These coordinates were used to determine bed profiles, volume of eroded material, and maximum depth of scour at instantaneous times.

Approximately 20–30 sediment concentration samples were collected in 2.5-L buckets at the flume exit per run. The time intervals between samples ranged from 30 s to 15 min, in a manner similar to photographic intervals. Each sample, of approximately 2000 mL, represents a concentration value averaged over a period of time that was greater for runs with lower flow rates (range approximately 4–11 s). Because the bed was steep (3.7%) and the reach downstream from the 40-cm test bed was armored with a plate, measured sediment concentration was seldom affected by either erosion or deposition downstream from the scour hole; however, there was a small delay between the time sediment exited the scour hole and was measured at the flume exit, corresponding to the time required to transport the sediment over the approximate 1-m length. The total sample volume was weighed to the nearest gram and allowed to settle for 24 h, after which the water was decanted. The remaining sample was allowed to evaporate at room temperature for an additional 24–48 h and weighed to the nearest 0.01 g. Sediment concentration was calculated by dividing the dry sediment weight by the difference between total sample and dry sediment weight. Details of the experimental setup, data collection, and run specifics are given in Stein (1990).

RESULTS

A total of 23 runs on three different bed materials were conducted in which the change in time of both sediment concentration and scour-hole geometry were measured. Typical scour profiles, in which the x -axis is parallel with the bed, for the cohesive soil (run 8) and fine sand $d_{50} = 0.15$ mm (run 26) over a period of approximately 2.5 h are shown in Figs. 3(a) and 3(b), respectively. Unlike these bed types, the coarse sand exhibited the shape noted by both Kobus et al. (1979) and Akashi and Saitou (1986) in which a steep-sided active scour hole is contained within a scour hole with sediment particles at the angle of repose. For all runs, maximum depth of scour is in the vicinity of the calculated centerline of the impinging jet, but, unlike results of Chee and Yuen (1985), this maximum is consistently shifted in the upstream direction. For most of the sand runs (but none of the cohesive-soil runs), a small mound of sediment developed just downstream from the scour hole at initial times, when detachment within the

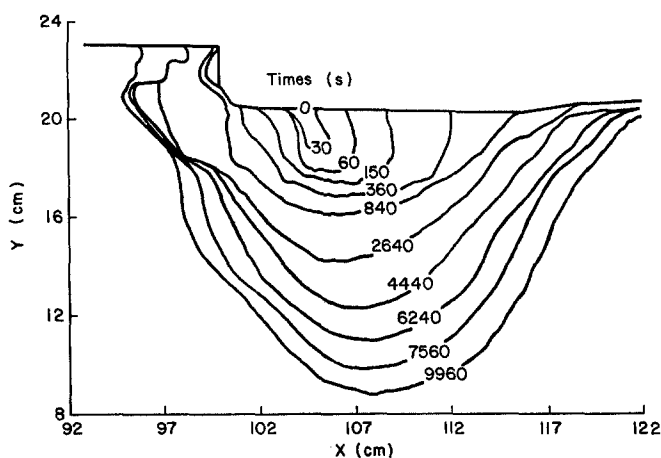


FIG. 3(a). Cohesive-Soil Scour Profiles versus Time

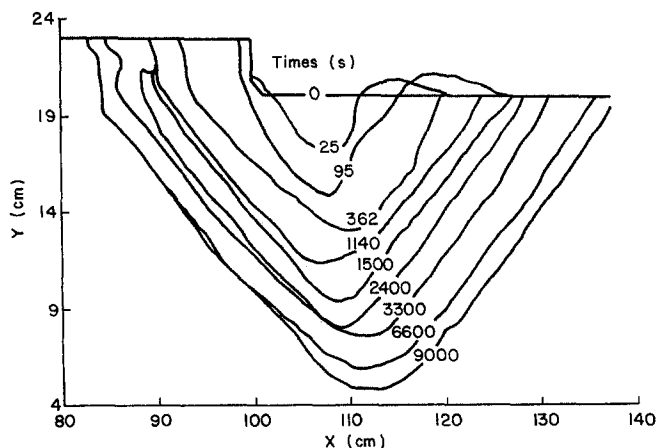


FIG. 3(b). Fine-Sand Scour Profiles versus Time

scour hole exceeded the downstream channel's sediment transport capacity [Fig. 3(b)]. As the scour hole grew larger and detachment capacity sufficiently decreased, the mound eroded and all sediment detached in the scour hole was transported to the flume exit. While the effect of the mound on tailwater depth and sediment concentration is not considered in the analysis, its effect is short-lived (less than 150 s).

A regression analysis of V^* versus D^* was performed to determine the shape function $\phi = \alpha \cdot \beta$ and exponent β . The resulting coefficients as well as bulk density B and the experimental sediment detachment parameters κ , ξ , and τ_c , which were independently determined from the scour-depth measurements (Stein and Julien 1991; Stein et al. 1993), are shown in Table 1. Two distinct shapes are noted for the coarse sand, dependent on the drop height creating the impinging jet, as could be expected from the analysis of Kobus et al. (1979). For a lower drop height, the active scour hole was less

TABLE 1. Experimental Scour Shape and Sediment-Detachment Parameters

Material (1)	α (2)	β (3)	κ^a (4)	ξ (5)	τ_c (Pa) (6)	B (kg/m ³) (7)
Coarse-sand shape 1	1.60	2.11	0.98	1.5	0.74	1,350
Coarse-sand shape 2	0.94	1.79	0.98	1.5	0.74	1,350
Fine sand	2.33	2.10	0.30	1.5	0.35	1,670
Cohesive soil	1.83	1.76	0.04	1.0	0.32	1,290

^aUnits dependent on value of ξ : κ in s/m if $\xi = 1.0$; κ in s²/m^{0.5}·kg^{0.5} if $\xi = 1.5$.

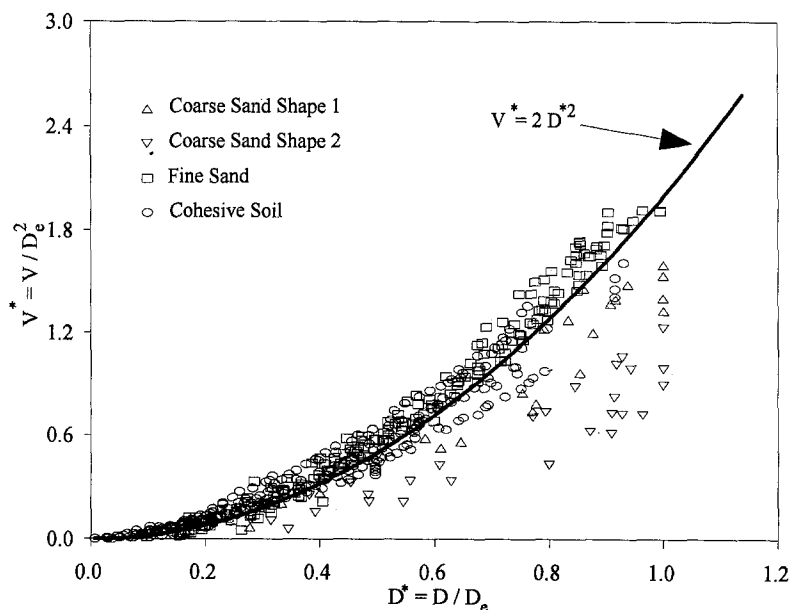


FIG. 4. Measured-Scour-Hole Volume versus Measured Depth

pronounced and the scour hole grew longer for a given depth. The fine-sand and cohesive-soil scour profiles were unaffected by drop height. From the regression coefficients, an assumption that $\alpha \approx \beta \approx 2$ —therefore $\phi \approx 4$ appears reasonably valid for all bed materials and scour-hole shapes, especially for the fine sand and cohesive soil. The data for all 23 runs, which include three different bed materials, are compared with the approximate assumption that $V^* = 2 \cdot D^{*2}$ in Fig. 4.

The pertinent hydraulic variables q , U_0 , y_0 , and χ and other normalizing parameters D_p , D_e , D_p^* , T_p , T_r , T_p^* , and C_{\max} required to compare sediment concentration, scour volume, scour depth, and time are given in Table 2. Jet velocity, thickness, and impingement angle were determined from a simple free-falling nappe relationship:

$$U_0 = \sqrt{u_e^2 + 2gh_d} \quad (22a)$$

$$y_0 = \frac{q}{U_0} \quad (22b)$$

$$\chi = \tan^{-1} \left(\frac{\sqrt{2gh_d}}{u_e} \right) \quad (22c)$$

where u_e = the velocity at the brink of the free overfall; g = the gravitational acceleration; and h_d = the drop height between the brink and downstream bed. A value of 2.6 was taken as the diffusion constant C_d . The coefficient of friction was determined from a Blasius flow assumption, i.e.

$$C_f = \frac{0.22}{8} \left(\frac{q}{\nu} \right)^{-0.25} \quad (23)$$

where q = unit discharge; ν = the kinematic viscosity; and q/ν = the Reynolds number.

Theoretical and experimental results of the relation between sediment concentration and time are compared for eight coarse-sand runs, six fine-sand runs and nine cohesive-soil runs in Figs. 5, 6, and 7, respectively. The theory is developed from a solution of (15) and (21) using normalizing parameters in Tables 1 and 2 plus $\beta = 2$ and $\phi = 4$. The depth of potential core scour $D_p^* = D_p/D_e$ varies slightly in the experiments from 0.06 to 0.15 for cohesive soil, 0.07 to 0.11 for fine sand, and 0.14 to 0.22 for the coarse sand. The term D_p^* influences solutions to (15), but as seen in Figs. 5–7 is insignificant within the experimental range.

For the runs with sand (Figs. 5 and 6), agreement between predicted and measured sediment concentration versus time is good throughout the entire scour process. Sediment concentration is near the predicted maximum initially, while scour is occurring within the potential core, and decreases as the scour hole and diffusion length of the impinging jet grows. The predicted maximum sediment concentration for the cohesive soil (Fig. 7) is considerably less than measured. At initial times for the cohesive-soil tests, measured sediment concentration values were unavoidably enhanced by additional scour in the test bed downstream from the free overfall. However, as the scour hole developed, the remaining test bed stabilized and the experimental conditions matched the theory developed in (15) and (21). At these longer scour times, theory approximates the measured sediment concentration, in a fashion similar to the sand runs. The time of potential core scour ($C \approx C_{\max}$) is very small, averaging 3.7, 10.6, and 135.0 s for the

TABLE 2. Experimental Hydraulic Parameters

Run (1)	$q \times 10^6$ ($m^3/s \cdot m$) (2)	U_0 (m/s) (3)	y_0 (mm) (4)	χ (5)	D_p (mm) (6)	D_c (mm) (7)	D_p^* (8)	T_p (s) (9)	T_r (s) (10)	T_p^* (11)	C_{max} (g/g) (12)
(a) Cohesive Soil $d_{50} = 0.045 \text{ mm}$											
13	1,570	0.6818	2.3	41	10	68	0.15	174	6,615	0.026	0.0017
12	4,890	0.9339	5.2	28	17	159	0.11	194	15,509	0.013	0.0014
7	1,540	0.8105	1.9	51	10	94	0.11	114	9,220	0.012	0.0026
3	2,250	0.8672	2.6	46	13	125	0.10	139	12,253	0.011	0.0024
11	3,460	0.9500	3.6	41	16	173	0.09	164	16,921	0.010	0.0022
6	4,500	1.0120	4.4	38	19	211	0.09	176	20,607	0.009	0.0020
8	1,720	1.0363	1.7	59	10	145	0.07	66	14,167	0.005	0.0037
10	3,540	1.1420	3.1	51	16	249	0.07	111	24,343	0.005	0.0031
9	4,580	1.1939	3.8	48	19	302	0.06	128	29,531	0.004	0.0029
(b) Coarse Sand $d_{50} = 1.5 \text{ mm}$											
21	1,620	0.8173	2.0	50	10	47	0.22	4	115	0.032	0.1274
20	2,570	0.8905	2.9	45	14	63	0.22	4	140	0.032	0.1166
19	3,470	0.9506	3.7	41	16	76	0.21	5	161	0.030	0.1122
18	4,930	1.0358	4.8	37	19	96	0.20	5	192	0.026	0.1093
14	1,680	1.0337	1.6	59	9	68	0.14	1	163	0.009	0.1176
15	2,350	1.0757	2.2	55	12	83	0.15	2	184	0.010	0.1064
16	3,530	1.1415	3.1	51	16	106	0.15	3	216	0.012	0.0933
17	4,800	1.2043	4.0	47	20	129	0.15	3	247	0.012	0.0899
(c) Fine Sand $d_{50} = 0.15 \text{ mm}$											
22	1,660	0.8206	2.0	50	10	99	0.11	10	2,837	0.003	0.0384
23	2,320	0.8724	2.7	46	13	122	0.11	14	3,354	0.004	0.0361
24	3,490	0.9518	3.7	41	16	161	0.10	16	4,172	0.004	0.0340
27	1,750	1.0383	1.7	59	10	140	0.07	5	3,858	0.001	0.0716
26	2,420	1.0799	2.2	55	12	172	0.07	7	4,433	0.002	0.0656
25	3,370	1.1331	3.0	51	16	212	0.07	9	5,155	0.002	0.0606

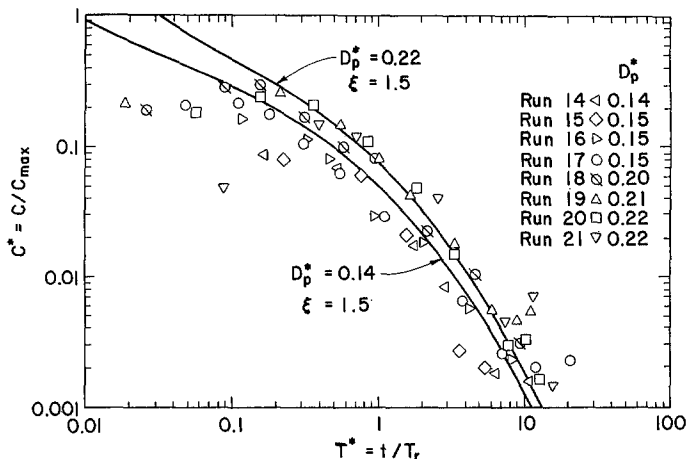


FIG. 5. Predicted versus Measured Sediment Concentration: Coarse Sand

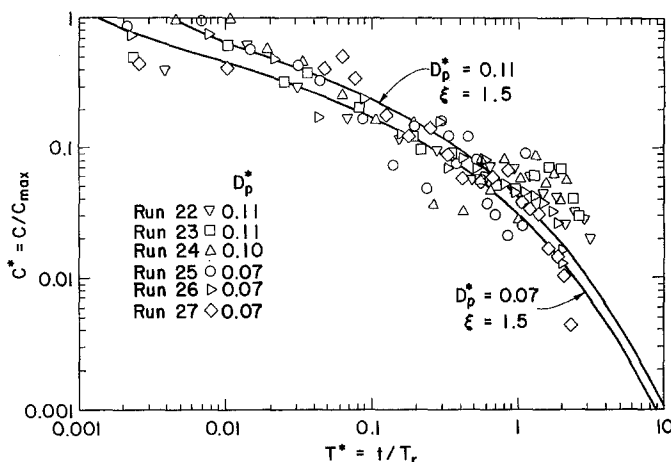


FIG. 6. Predicted versus Measured Sediment Concentration: Fine Sand

coarse sand, fine sand, and cohesive soil, respectively. Also, agreement between measured sediment concentration and time is enhanced for all cases if the regression coefficients in Table 1 are used rather than using $\beta = 2$ and $\phi = 4$. However, use of the approximate values allows a common shape factor to be used for all bed materials while still maintaining an acceptable accuracy level.

PROCEDURE

The following example illustrates the procedure for the calculation of sediment concentration and scour geometry changes with time.

The parameters are: flow such that $U_0 = 1.19$ m/s, $y_0 = 0.0021$ m, and $\chi = 65^\circ$ (as would be caused by a $0.0025\text{-m}^2/\text{s}$ flow approaching a 6-cm drop at 0.5 m/s); and the bed material is sand, $d_{50} = 0.15$ mm, such that $\kappa =$

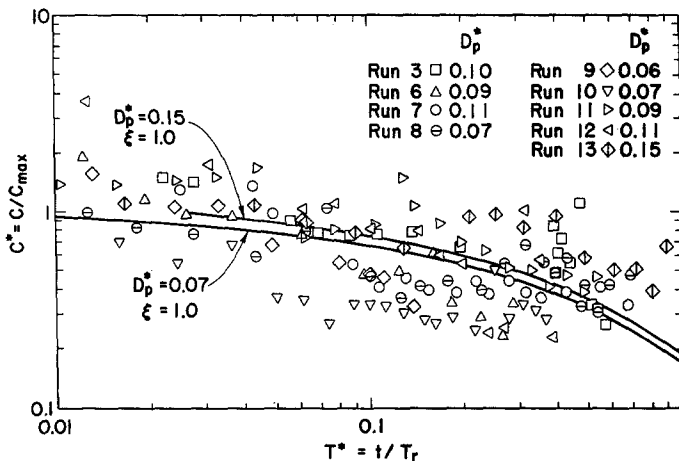


FIG. 7. Predicted versus Measured Sediment Concentration: Cohesive Soil

$0.30 \text{ s}^2/\text{kg}^{0.5} \cdot \text{m}^{0.5}$, $\xi = 1.5$, and $\tau_c = 0.35 \text{ N/m}^2$, with a bulk density of $1,900 \text{ kg/m}^3$. (See Table 1 for parameter ranges.)

The following must be determined: the expected equilibrium scour depth, the maximum sediment concentration, the sediment concentration when the scour depth is 0.1 m , and the sediment concentration at $t = 5 \text{ min} = 300 \text{ s}$.

Solution

Expected Equilibrium Scour Depth

From (23), calculate the coefficient of friction:

$$C_f = \frac{0.22}{8} \left(\frac{0.0025}{1 \times 10^{-6}} \right)^{-0.25} = 0.0039 \quad (24)$$

From (6), calculate the maximum applied shear stress:

$$\tau_0 = 0.0039 \times \frac{1,000 \text{ kg}}{\text{m}^3} \times \frac{1.19^2 \text{ m}^2}{\text{s}^2} = \frac{5.52 \text{ N}}{\text{m}^2} \quad (25)$$

From (8) and assuming $C_d = 2.6$, calculate the equilibrium scour depth:

$$D_e = \frac{2.6^2 \times 0.0039 \times \frac{1,000 \text{ kg}}{\text{m}^3} \times \frac{1.19^2 \text{ m}^2}{\text{s}^2} \times 0.0021 \text{ m}}{\frac{0.35 \text{ kg}}{\text{ms}^2}} \sin 65^\circ = 0.20 \text{ m} \quad (26)$$

Maximum Sediment Concentration

From (9), calculate the potential core scour depth:

$$D_p = 2.6^2 \times 0.0021 \text{ m} \times \sin 65^\circ = 0.013 \text{ m} \quad (27a)$$

$$D_p^* = \frac{0.013 \text{ m}}{0.20 \text{ m}} = 0.065 \quad (27b)$$

From (20) and taking $\phi = 4$ and $\beta = 2$, calculate the maximum sediment concentration:

$$C_{\max} = \frac{\frac{0.30 \text{ s}^2}{\text{kg}^{0.5} \text{ m}^{0.5}} \times 0.20 \text{ m} \times \frac{0.35^{1.5} \text{ kg}^{1.5}}{\text{m}^{1.5} \text{ s}^3}}{\frac{1,000 \text{ kg}}{\text{m}^3} \times \frac{0.0025 \text{ m}^2}{\text{s}}} \times 4 \times 0.065 \times \left(\frac{1 - 0.065}{0.065} \right)^{1.5} = \frac{0.071 \text{ g sediment}}{1 \text{ g water}} \quad (28)$$

Assuming the specific weight of sediment is 2.65, sediment concentration expressed in milligrams per liter is:

$$C_{\max} = \frac{10^6 \times 2.65 \times 0.071}{2.65 + 0.071} = \frac{69,100 \text{ mg}}{\text{L}} \quad (29)$$

Sediment Concentration with 0.1-m Scour Depth

Check that $D > D_p$ ($0.1 \text{ m} > 0.013 \text{ m}$; yes) and calculate D^* :

$$D^* = \frac{0.1 \text{ m}}{0.20 \text{ m}} = 0.50 \quad (30)$$

From (14), calculate the reference time:

$$T_r = \frac{\frac{1,900 \text{ kg}}{\text{m}^3} \times 0.20 \text{ m}}{\frac{0.30 \text{ s}^2}{\text{kg}^{0.5} \text{ m}^{0.5}} \times \frac{0.35^{1.5} \text{ kg}^{1.5}}{\text{m}^{1.5} \text{ s}^3}} = 6,120 \text{ s} \quad (31)$$

From (11), calculate the time of potential core scour:

$$T_p = \frac{\frac{1,900 \text{ kg}}{\text{m}^3} \times 0.013 \text{ m}}{\frac{0.30 \text{ s}^2}{\text{kg}^{0.5} \text{ m}^{0.5}} \times (5.52 - 0.35)^{1.5} \frac{\text{kg}^{1.5}}{\text{m}^{1.5} \text{ s}^3}} = 7.00 \text{ s} \quad (32)$$

From (21), calculate the sediment concentration:

$$\frac{C}{C_{\max}} = \left(\frac{0.065}{0.50} \right)^{0.5} \left(\frac{1 - 0.50}{1 - 0.065} \right)^{1.5} = 0.14 \quad (33a)$$

$$C = 0.14 \times 0.071 = \frac{0.0099 \text{ g sediment}}{1 \text{ g water}} = \frac{9,860 \text{ mg}}{\text{L}} \quad \text{when } D = 0.1 \text{ m} \quad (33b)$$

Sediment Concentration at $t = 5 \text{ min}$

Check that $t > T_p$ ($300 \text{ s} > 7.0 \text{ s}$; yes) and calculate T^* :

$$T^* = \frac{300 \text{ s}}{6,120 \text{ s}} = 0.049 \quad (34)$$

From Fig. 6 with $D_p^* = 0.065$ and $T^* = 0.049$, read $C^* = 0.25$; therefore

$$C = 0.25 \times 0.071 = \frac{0.018 \text{ g sediment}}{1 \text{ g water}} = \frac{17,300 \text{ mg}}{\text{L}} \quad \text{when } t = 300 \text{ s} \quad (35)$$

Alternatively, with $D_p^* = 0.065$ and $T^* = 0.049$, solve (15b) iteratively for D^* and use (21) to solve for concentration.

CONCLUSIONS

The sediment concentration exiting a scour hole below a free overfall is directly related to the sediment detachment potential of a jet impinging on an erodible bed. At any given time, sediment concentration is directly related to the corresponding maximum scour depth as shown in (19). When the eroding bed is within the impinging jet's potential core, concentration is near a maximum as given in (20). Thereafter, concentration decreases with depth as given by (21). Sediment concentration also decreases with time as expressed in (15) and (21) and shown in Figs. 5–7.

The validity of the relationships between sediment concentration and time, developed in (15) and (19)–(21), is tested in the laboratory with noncohesive and cohesive bed materials. Agreement between measured and predicted sediment concentration is good throughout the scour process when scour occurs in noncohesive soils, as shown in Figs. 5 and 6. For the case of scour in cohesive soils, theory approximates experimental results at longer times, as shown in Fig. 7. The shape of the scour hole influences the relationships between sediment concentration and scour depth [(21)] and sediment concentration and time (Figs. 5–7). An assumption that the scour-hole volume per unit width is twice the square of scour depth at the corresponding time is shown to be reasonably valid for all bed materials in Fig. 4.

ACKNOWLEDGMENTS

This study has been primarily funded by the U.S. Department of Agriculture–Agricultural Research Service's Great Plains Research Group. Additional support is provided by the Army Research Office Center for Geosciences at Colorado State University (grant ARO/DAAL 03-86-K-0175) and the Montana State Agricultural Experiment Station (paper J-2869). Our appreciation is extended to all groups.

APPENDIX I. REFERENCES

- Albertson, M. L., Dai, Y. B., Johnson, R. A., and Rouse, H. (1950). "Diffusion of submerged jets." *Trans.*, ASCE, 115, 639–697.
- Akashi, N., and Saitou, T. (1986). "Influence of water surface on scour from a vertical submerged jet." *J. Hydraul. and Hydr. Engrg.*, 4(2), 55–69.
- Begin, Z. B., Meyer, D. F., and Schumm, S. A. (1980a). "Knickpoint migration due to base level lowering." *J. Waterway, Port., Coast. and Oc. Div.*, ASCE, 106(3), 369–389.
- Begin, Z. B., Meyer, D. F., and Schumm, S. A. (1980b). "Sediment production of

- alluvial channels in response to base level lowering." *Trans.*, American Society of Agricultural Engineers, 23(5), 1183–1188.
- Beltaos, S. (1972). "Normal impingement of plane turbulent jets on sooth walls," MS thesis, University of Alberta, at Edmonton, Alberta.
- Beltaos, S. (1974). "Turbulent impinging jets," PhD dissertation, University of Alberta, at Edmonton, Alberta.
- Beltaos, S. (1976). "Oblique impingement of plane turbulent jets." *J. Hydr. Div.*, ASCE, 102(9), 1177–1192.
- Beltaos, S., and Rajaratnam, N. (1973). "Plane turbulent impinging jets." *J. Hydr. Res.*, 11(1), 29–59.
- Blaisdell, F. W., and Anderson, C. L. (1988a). "A comprehensive generalized study of scour at cantilevered pipe outlets, Pt. 1." *J. Hydr. Res.*, 26(4), 357–376.
- Blaisdell, F. W., and Anderson, C. L. (1988b). "A comprehensive generalized study of scour at cantilevered pipe outlets, Pt. 2." *J. Hydr. Res.*, 26(5), 509–524.
- Blaisdell, F. W., Anderson, C. L., and Hebaus, G. G. (1981). "Ultimate dimensions of local scour." *J. Hydr. Div.*, ASCE, 107(3), 327–337.
- Bormann, N. E., and Julien, P. Y. (1991). "Scour downstream of grade control structures." *J. Hydr. Engrg.*, ASCE, 117(5), 597–594.
- Chee, S. P., and Kung, T. (1971). "Stable profiles of plunge basins." *Water Res. Bull.*, 7(2), 303–308.
- Chee, S. P., and Yuen, E. M. (1985). "Erosion of unconsolidated gravel beds." *Can. J. Civ. Engrg.*, 12(3), 559–566.
- Foster, G. R., Meyer, L. D., and Onstad, C. A. (1977). "An erosion equation derived from basic erosion principles." *Trans.*, American Society of Agricultural Engineers, 20(4), 678–682.
- Gardner, T. W. (1983). "Experimental study of knickpoint and longitudinal profile in cohesive, homogeneous material." *Geol. Soc. Amr. Bull.*, 94(5), 664–672.
- Hanson, G. J. (1989). "Channel erosion study of two compacted clays." *Trans.*, American Society of Agricultural Engineers, 32(5), 485–490.
- Holland, W. N., and Pickup, G. (1976). "Flume study of knickpoint development in stratified sediment." *Geol. Soc. Amr. Bull.*, 87(1), 76–82.
- Kobus, H., Liester, P., and Westrich, B. (1979). "Flow field and scouring effects of steady and pulsating jets impinging on a moveable bed." *J. Hydr. Res.*, 17(3), 175–192.
- Laursen, E. M. (1952). "Observations on the nature of scour." *Proc. 5th Hydr. Conf.*, University of Iowa, Iowa City, Iowa, 179–197.
- Mason, P. J., and Arumugam, K. (1985). "Free jet scour below dams and flip buckets." *J. Hydr. Engrg.*, ASCE, 111(2), 220–235.
- Nearing, M. A., Foster, G. R., Lane, L. J., and Finkner, S. A. (1989). "A process-based soil erosion model for USDA water erosion prediction project technology." *Trans.*, American Society of Agricultural Engineers, 32(5), 1587–1593.
- Rajaratnam, N. (1976). "Turbulent jets." *Development in Water Science 5*. Elsevier Scientific Publishing Co., Amsterdam, the Netherlands.
- Rajaratnam, N. (1981). "Erosion by plane turbulent jets." *J. Hydr. Res.*, 19(4), 339–359.
- Rajaratnam, N. (1982). "Erosion by unsubmerged plane water jets." *Proc. Applying research to hydraulic practice*, ASCE, New York, N.Y., 280–288.
- Robinson, K. M. (1989a). "Hydraulic stress on an overfall bounday." *Trans.*, American Society of Agricultural Engineers, 32(4), 1269–1274.
- Robinson, K. M. (1989b). "Stress distribution at an overfall." *Trans.*, American Society of Agricultural Engineers, 32(1), 75–80.
- Rouse, H. (1940). "Criteria for similarity in the transportation of sediment." *Proc. 1st Hydraulic Conf.*, State University of Iowa, Iowa City, Iowa, 33–49.
- Stein, O. R. (1990). "Mechanics of headcut migration in rills," PhD dissertation, Colorado State University, at Fort Collins, Colo.
- Stein, O. R., and Julien, P. Y. (1991). "Measurement of rill erosion sediment detachment." *Paper No. 91-2086*, American Society of Agricultural Engineers, St. Joseph, Mo.

- Stein, O. R., and Julien, P. Y. (1993). "A criterion delineating the mode of headcut migration." *J. Hydr. Engrg.*, ASCE, 119(1), 37–50.
- Stein, O. R., Julien, P. Y., and Alonso, C. V. (1993). "Mechanics of jet scour downstream of a headcut." *J. Hydr. Res.*, 31(6), 723–738.

APPENDIX II. NOTATION

The following symbols are used in this paper:

- B = soil bulk density;
 C = sediment concentration;
 C_d = diffusion constant of jet;
 C_f = coefficient of friction;
 C_{\max} = sediment concentration at tip of potential core;
 D = maximum depth of jet scour at given time t ;
 D^* = normalized scour depth (D/D_e);
 D_e = equilibrium depth of jet scour;
 D_p = depth of scour corresponding to potential core tip;
 D_p^* = normalized depth of potential core tip (D_p/D_e);
 d_{50} = mean sediment size;
 E = sediment detachment rate per unit area;
 g = gravitational acceleration;
 h_d = drop height;
 h_t = tailwater depth;
 J = distance along jet centerline;
 J_e = distance along jet centerline to impingement at equilibrium;
 J_p = length of jet potential core;
 q = unit-flow discharge;
 T^* = normalized time (t/T_r);
 T_p = time of potential core scour;
 T_p^* = normalized time of potential core score (T_p/T_r);
 T_r = reference time;
 t = time;
 u_e = velocity at the brink of overfall;
 U = maximum diffused jet velocity;
 U_0 = initial jet velocity;
 V = scour-hole volume;
 V^* = normalized scour-hole volume (V/D_e^*2);
 y_0 = initial jet thickness;
 α, β = experimental scour-shape factors;
 κ, ξ = experimental parameters of sediment-detachment function;
 ν = fluid kinematic viscosity;
 ρ = fluid density;
 τ_c = critical shear stress for erosion initiation;
 τ = shear stress in scour hole;
 τ_0 = shear stress in potential core;
 ϕ = scour-hole shape factor = $\alpha \cdot \beta$; and
 χ = jet angle at tailwater impingement.